THE ASTROPHYSICAL JOURNAL, 473:L107–L110, 1996 December 20

ROSSI X-RAY TIMING EXPLORER OBSERVATIONS OF GRS 1915+105

J. GREINER
Max-Planck-Institut für extraterrestrische Physik, 85740 Garching, Germany
AND
E. H. MORGAN AND R. A. REMILLARD
Center for Space Research, Massachusetts Institute of Technology, Cambridge, MA 02139
Received 1996 July 5; accepted 1996 October 4

ABSTRACT

The Galactic superluminal motion source GRS 1915+105 was observed with the *Rossi X-Ray Timing Explorer* satellite at several occasions during its ongoing active state. The observed X-ray intensity changes drastically on a variety of timescales ranging from subseconds to days. In particular, the source exhibits quasi-periodic brightness sputters with varying duration and repetition timescale. These episodes occur occasionally, while the more common X-ray intensity variations are faster with much smaller amplitudes. The spectrum during the brightness sputters is remarkably different from the spectrum of the mean high-state emission. We argue that such sputtering episodes are possibly caused by a major accretion disk instability. Based on the coincidence in time of two radio flares following the observed X-ray sputtering episodes, we speculate that superluminal ejections (as observed from GRS 1915+105 during earlier activity periods) are related to episodes of large-amplitude X-ray variations.
Subject headings: accretion, accretion disks — instabilities — stars: individual (GRS 1915+105) — X-rays: stars

1. INTRODUCTION

On 1992 August 15 the WATCH detectors on *Granat* discovered a new X-ray transient (Castro-Tirado, Brandt, & Lund 1992), which was designated GRS 1915+105. Follow-up monitoring with WATCH and BATSE (Harmon, Paciesas, & Fishman 1992) revealed an unusual light curve consisting of a 3 month rise, an 8 month high-intensity plateau phase, and a 2 month decline. A variable radio source was found with the VLA (Mirabel et al. 1993a) inside the ±10″ X-ray error circle (Greiner 1993), as well as a variable infrared source (Mirabel et al. 1993b; Castro-Tirado et al. 1993). The soft X-ray spectrum as seen with the *ROSAT* PSPC on several occasions is strongly absorbed ($N_{\rm H} \approx 5 \times 10^{22}$ cm^{-2}; Greiner 1993), which supports the earlier conjecture that GRS 1915+105 is located behind the Sagittarius arm, i.e., at a distance greater than 8 kpc (Greiner et al. 1994). Indeed, later H I measurements suggest a distance of about 12.5 kpc (Mirabel & Rodríguez 1994). The optical counterpart (at the radio position) was only detected in the *I* band at 23.4 mag, while it is fainter than 25.9, 26.1, and 26.1 mag in *B*, *V*, and *R*, respectively (Boër, Greiner, & Motch 1996).

An outburst with a light curve similar to the one described above (but with shorter duration) occurred between 1993 December and 1994 April, at which time GRS 1915+105 was observed in a remarkably high radio state. Further radio monitoring revealed radio structures traveling at apparently superluminal speed (Mirabel & Rodríguez 1994), which made GRS 1915+105 the first superluminal source in the Galaxy. Until then, apparent superluminal motion was observed only in active galactic nuclei, the central engines of which are generally believed to be massive black holes. This similarity suggests that GRS 1915+105 harbors a stellar-sized black hole. Indirect support for this hypothesis was provided by the discovery of the second Galactic superluminal motion source GRO J1655−40 (Zhang et al. 1994), for which a mass function larger than 3 $M_\odot$ was subsequently established by optical radial velocity measurements (Bailyn et al. 1995).

2. ALL-SKY MONITOR DISCOVERY OF RENEWED ACTIVITY IN GRS 1915+105

The *Rossi X-Ray Timing Explorer* (*RXTE*) all-sky monitor (ASM) observes bright X-ray sources in the range of ~2 to 12 keV using position-sensitive proportional counters placed below coded masks. X-ray intensity measurements are derived from the deconvolution of overlapping mask shadows from each X-ray source in a camera's field of view. There are three Shadow Scanning Cameras (SSCs) in the ASM, and the field of view of each camera is 6° × 90° FWHM. Histograms of detected counts versus anode wire position are telemetered for each SSC in three separate energy bands (1.3–3.0, 3.0–4.8, and 4.8–12.2 keV). Detector problems were experienced soon after launch, but performance was stabilized with an operating duty cycle of ~40% (limited to low-background regions of the *RXTE* orbit). This data rate provides approximately seven celestial scans per day, with sky coverage obtained in a series of 90 s stationary exposures ("dwells") followed by an instrument rotation of 6°. Data collection has been ongoing with at least one SSC since 1996 February 21.

The data analysis utilizes all eight anode wires in SSC1 and six anode wires in each of SSC2 and SSC3. The fine details of the instrument calibration are still being refined, and the present analysis is subject to a systematic error of about 3% for uncrowded source regions (such as that around GRS 1915+105), as inferred from the rms deviations observed in the Crab Nebula. Further details of the instrument and the data analysis methods are provided by Levine et al. (1996). For the ASM observations of GRS 1915+105 reported below, we select results from individual SSC dwells and normalize all of the results to the throughput of SSC1, in which the Crab yields a total count rate of 73 SSC counts s^{-1}. For the present investigation, we exclude measurements in which the angle between the X-ray source and Earth is less than 75°. We also exclude observations in which a camera's field of view contains more than 15 potential X-ray sources or observations in which any two sources are within a rectangle of $0\overset{\circ}{.}1 \times 6\overset{\circ}{.}0$ aligned perpendicular to the anode wires.

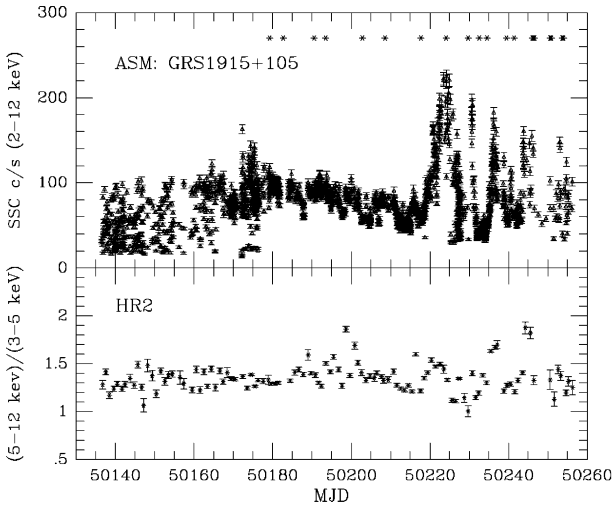

FIG. 1.—Light curve of GRS 1915+105 as measured with the *RXTE*/ASM in the 2–12 keV range (*top panel*) and spectral hardness ratio, defined as HR2 = flux (5–12 keV)/flux (3–5 keV) (*bottom*).

The ASM light curve for the period 1996 February 21 to June 21 is shown in Figure 1. Extreme and evolving levels of X-ray variability were confirmed by the appearance of rapid variations (seconds to minutes) seen in the ASM time series data (collected in parallel with position histogram data) during many dwells when GRS 1915+105 was in an SSC field of view. An ASM alert led to *RXTE* pointed observations with the proportional counter array (PCA) and High Energy X-Ray Timing Experiment (HEXTE) instruments. The times of the pointed observations are marked with an asterisk in the top panel of Figure 1.

3. POINTED *RXTE* OBSERVATIONS

The PCA on *RXTE* (Zhang et al. 1993) consists of five nearly identical xenon-filled proportional counter units (PCUs), each with 1250 cm^2 of collecting area. The detectors are sensitive to X-rays between 2 and 60 keV with 17% energy resolution at 6 keV. The Crab produces 2500 counts s^{-1} per PCU (2–60 keV), while the background count rate is typically ~20 counts s^{-1} per PCU. On April 6, April 9, April 17, and May 14, only three PCUs were used because of an operational problem. On April 15, the gain of all five PCUs was lowered by 30%. Owing to the steep energy spectrum (see below), we discuss the PCA but not the HEXTE data in this short communication.

3.1. *Temporal Characteristics*

The X-ray light curves reveal a variety of features, one of which is large-amplitude intensity variations. This is very similar to the behavior seen from dwell to dwell in the ASM, as well as in the light curves of individual dwells.

We identify the following properties in the light curves of GRS 1915+105 (see Figs. 2, 3, and 4):

Repeating pattern of brightness sputters.—In five of the pointed PCA observations (April 6, May 21, May 26, June 16, and June 19), we find large, eclipse-like dips in the X-ray flux, which we call sputters. During these sputters, the flux drops from ≈2–3 crab to a momentary lull at about 100–500 mcrab and then shoots up again. The spectrum softens dramatically during the brightness sputters. The sputters occur quasi-periodically with a recurrence time of about 250 s during the first observation (see Fig. 3, *top*). The decline to the low level

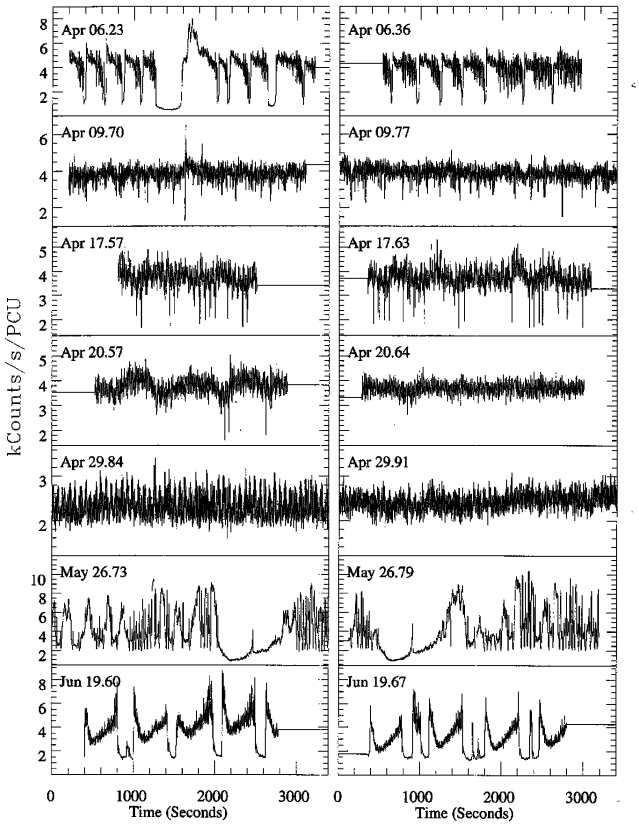

FIG. 2.—Light curves of GRS 1915+105 as measured with the *RXTE*/PCA (2–60 keV range, but dominated by photons below 25 keV owing to the spectral shape). Shown is the count rate per PCU (note the different scales) at 1 s time resolution, with each panel showing one orbit of selected pointed observations. All the variations in X-ray count rate are due to GRS 1915+105, i.e., Earth occultations and SAA passages are removed, while dead time is negligible and has not been corrected for (which is 1% per 1000 counts s^{-1} per PCU).

(lull) typically takes 3–5 s, and the rise to the high level typically takes 5–10 s. The lull duration varies irregularly, with a mean value of between 30 and 50 s during the first observation and only a few seconds in later observations. The low-intensity value during the lull is surprisingly constant with time during the first observations. It is also interesting to note that the rms variability during the brightness sputters is much smaller than elsewhere. During the June 16 and June 19 observations, the brightness sputters all have a small flare lasting 10 s at the start of the sputter.

Large-amplitude oscillations.—On April 6, the X-ray intensity starts oscillating with increasing amplitude toward the lull, with the last oscillation before the lull nearly reaching the low-intensity level of the lull (Fig. 3). On May 26, we see extremely large amplitude oscillations with an amplitude of nearly 3 crab and periods of 30–100 s.

Flare following lull.—On one occasion on April 6, the intensity remained low for over 300 s, and there is a large (to >3 crab) flare following this lull that is spectrally invariable, in sharp contrast to the spectral softening seen during the brightness sputters. After the flare, there is a long delay before sputtering resumes (Fig. 2, *top*).

Brief flares in prolonged lulls.—During a major lull observed on May 26 (see Fig. 4), the source exhibited a flare lasting 5 s. Before this flare, the intensity went below the QPO floor.

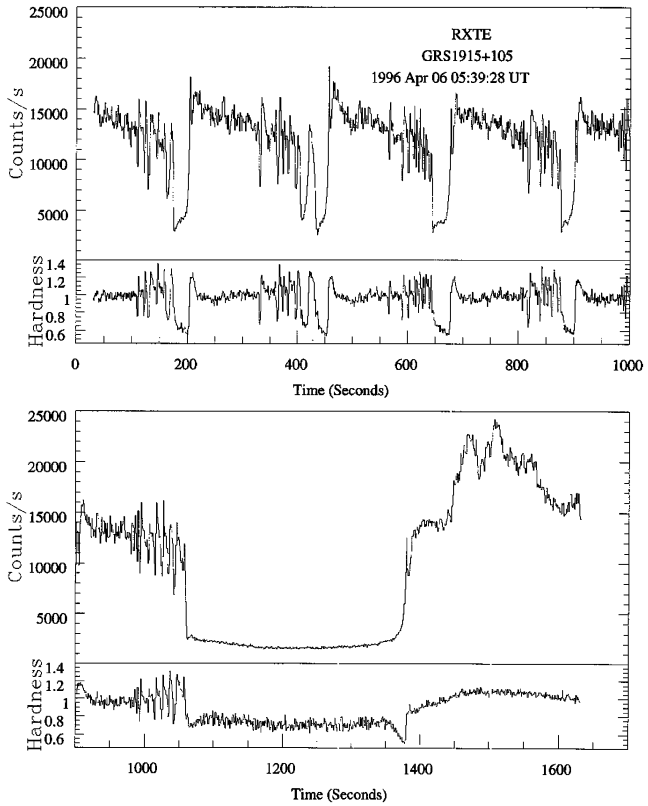

FIG. 3.—Blowup of a part of the light curve of GRS 1915+105 on 1996 April 6, showing the quasi-periodically repeating pattern of 30 s duration brightness sputters (*top*) and the major lull (*bottom*). The top panel of each plot shows the count rate per PCU, while the lower panel shows the hardness ratio (count ratio in the 4.4–25 vs. 2–4.4 keV band) at the same time resolution of 1 s (time along the abscissa refers to the time labeled in the top panel). Note the overshooting after the rebound and the long waiting time until sputtering resumes. Even during the lull, the background rate (about 5 counts s^{-1}) is still negligible as compared to the source rate.

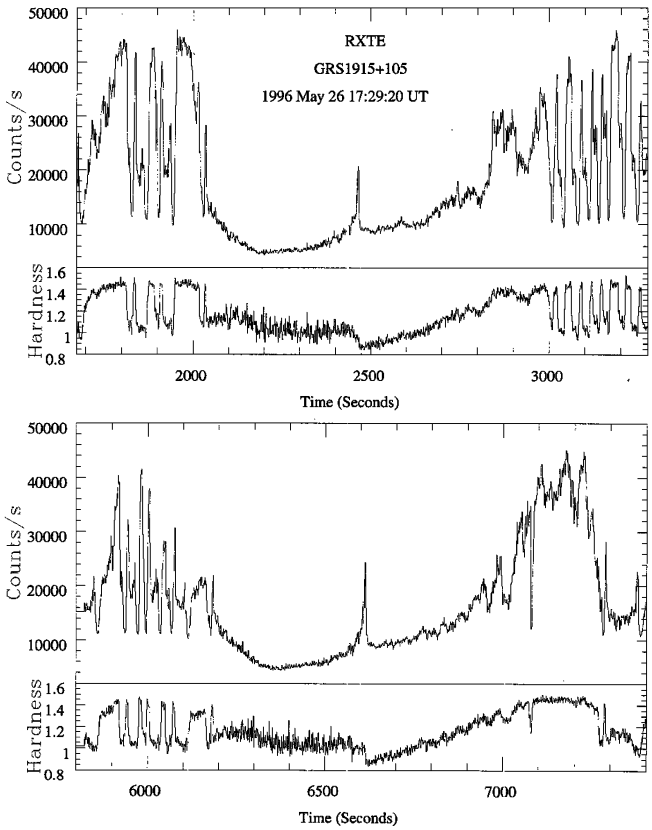

FIG. 4.—Blowup of a part of the light curve of GRS 1915+105 on 1996 May 26. The top panel of each plot shows the 2–25 keV count rate in one PCU, while the lower panel shows the hardness ratio (count ratio in the 4.4–25 vs. 2–4.4 keV band) at the same time resolution of 1 s.

About 400 s later, another sharp flare occurs as the source intensity climbs back up. This complex pattern is repeated almost identically 4925 s later (Fig. 4). Unfortunately, the observation ended before we could see if the pattern repeated more than twice.

Fast oscillations.—Between the episodes of large-amplitude variations, the variations are more regular, developing into clearly visible quasi-periodic oscillations (20 mHz–67 Hz) that have rich phenomenology including spectral characteristics and dynamically changing amplitudes and frequencies. These features will be discussed in a subsequent paper (Morgan, Remillard, & Greiner 1996).

The ASM light curve of GRS 1915+105 is marked by an interval of extreme and random variations that were in progress on February 21 and continued until April 7 (MJD 50,180; see Fig. 1). A later period that can be characterized as a series of X-ray flares (hours to days) occurred from May 17 to July 16 (MJD 50220–50280), and this interval was followed by 25 days of apparently steady emission at 0.51 crab. The PCA observations with highest amplitudes of both X-ray flux and variability occurred on April 6, May 20–26, and June 11–19, and these sample both the intervals of random variability and X-ray flaring seen with the ASM. A more detailed analysis of the temporal evolution of the quasi-periodic oscillations and their energy dependence are presented in a forthcoming paper (Morgan et al. 1996).

3.2. *Spectral Characteristics*

While a complete spectral analysis is beyond the scope of this Letter, a few general features can already be deduced at this early stage. The spectra during the April 9–29 observations are complex and rapidly variable. Most of these spectra are rather steep and fall off beyond 20 keV.

The hardness ratio panels in Figures 3 and 4 already demonstrate that the spectrum of the X-ray emission during the lulls is softer than during the high-intensity states, i.e., these lulls are not caused by absorption or any low-energy cutoff. We have selected photons (for individual layers and single PCA units using the ftools command saextrct) at different time intervals corresponding to these two intensity states. Slew data at the end of the observation were used for background subtraction, and the spectral fitting was done using the XSPEC package (Shafer et al. 1991). The gross energy distribution of the high-intensity emission (on April 6) can be described by a power-law model with photon index $\alpha = -1.6$ and a high-energy cutoff around 5 keV, while the high-intensity spectra on May 20 and 26 require a second component above $\approx$15 keV. The spectrum during the lulls (April 6 and May 26) is well represented by a two-component model, i.e., a disk blackbody plus a power law with photon index $\alpha = -2.2$ without a high-energy cutoff. The spectrum during the rebound is an extremely steep pure power law ($\alpha \approx$

−4.5). As can be inferred from the hardness ratio plot, there are no major spectral changes during the decay phase between lulls before the onset of the large-amplitude oscillations. But during these oscillations, the spectrum gets harder and softer than the mean on the same timescale as the oscillations.

4. DISCUSSION

The previously known properties of GRS 1915+105 had signified an unusual nature, compared to the known types of high-energy transients: the relativistic radio jets, slow rise time, and the spectral characteristics, as well as the lack of a systematic flux decay, are markedly different from black hole transients such as, e.g., GRS 1124−68 or GRO J0422+32. With our data from *RXTE* observations of GRS 1915+105, these differences are even more pronounced.

The absence of pulsed emission (Morgan et al. 1996) suggests that the observed X-ray emission does not come directly from the surface of a rotating, magnetic compact object. On the other hand, the strong variability during the high-intensity states on timescales well below 1 s indicates that the emission region cannot be a large and hot corona. We therefore tentatively assign this emission to an accretion disk.

GRS 1915+105 as observed in 1996 April with *RXTE* is at least a factor of 3 more intense than it was when observed by *ROSAT* (Greiner et al. 1994) and *ASCA* (Nagase et al. 1994; Ebisawa & White 1995) during previous active states. At a distance of GRS 1915+105 of 12.5 kpc (Mirabel & Rodríguez 1994), the mean, unabsorbed luminosity in the 1–25 keV range is of the order of 10^{39} ergs s^{-1} during the high-intensity states (a factor of 3 more than has been noted previously; see, e.g., Sazonov & Sunyaev 1996). This is well above the Eddington luminosity for a neutron star with any reasonable mass, which suggests that the system contains a black hole.

As evidenced by the energy spectra (softening), the brightness sputters are not absorption dips. Occultation events are unlikely for two reasons: First, the occulting body would have to be large in comparison to the projected X-ray–emitting area (in order to explain the short rise and fall times), which is difficult to reconcile if the emitting area is an accretion disk, even if only a fraction of the disk dominates the emission. Second, unless such an occulter were related to the large-amplitude oscillations in the X-ray flux, there is no reason to have the intensity drops always occur during times following large-amplitude oscillations. It is therefore more plausible to relate the large-amplitude oscillations as well as the sputters to a single phenomenon, e.g., an accretion disk instability. This is supported by the fact that the large-amplitude oscillations show similar spectral changes as the sputters.

If one relates the strongly variable X-ray emission to the inner part of an accretion disk, then, since the spectrum during the lulls is markedly different, one has to suppose that the inner part of the accretion disk is changed drastically. The accretion flow in the inner regions of an accretion disk around a compact object has been thought to undergo a sonic transition before falling supersonically onto the compact object (Matsumoto, Kato, & Fukue 1985). As the inner accretion disk is refilled rather quickly, it is certainly always far from being in a steady state. In fact, the observed X-ray spectrum in the 2–20 keV range is completely dissimilar to a steady, multicolor disk blackbody except during the lulls.

It is worth noting that the rebound after lulls does not correspond to the release of energy that is "missing" over the lull duration. This suggests that the energy is channeled into a different energy form, possibly kinetic. Episodes of large-amplitude variations (= major instabilities in our interpretation) have been observed on 1996 April 6 and May 20 and 26 as well as June 16 and 19 (Fig. 2). Interestingly, these times coincide with radio flares (with a delay between 1 and 5 days) reported for the period of May 23-26 (Pooley 1996) and another flare during June 17–22 (G. Pooley, private communication). Therefore, the episodes of large-amplitude X-ray variations may be related to the formation of jets. We also note that during these episodes, the X-ray spectrum shows a distinct hard component (though varying) that seems to be missing at other times. This component might permit the detection of GRS 1915+105 by BATSE (see Zhang et al. 1996 for the May 20–26 period). Previous radio monitoring of GRS 1915+105 and GRO J1655−40 has resulted in the perplexing result that not all X-ray active states were accompanied by radio emission (e.g., the 1995 April and August activity period of GRO J1655−40; Foster et al. 1996), which suggests that radio emission (jets) is not related simply to X-ray high states. If radio emission is correlated with episodes of large-amplitude, erratic X-ray variations later on subsequent occasions, the clue may have been found to relate jet formation to X-ray behavior.

We thank an anonymous referee for careful reading and detailed comments. J. G. is supported by the German Bundesministerium für Bildung, Wissenschaft, Forschung, und Technologie (BMBF/DARA) under contract No. FKZ 50 OR 9201. E. H. M. and R. R. were supported by NASA contract NAS5-30612. J. G. thanks the Deutsche Forschungsgemeinschaft (DFG) for a travel grant and is extremely grateful to H. Bradt and R. Vanderspek for their kind hospitality at MIT where most of this work was done.

REFERENCES

Bailyn, C. D., Orosz, J. A., McClintock, J. E., & Remillard, R. A. 1995, Nature, 378, 157
Boër, M., Greiner, J., & Motch, C. 1996, A&A, 305, 835
Castro-Tirado, A. J., Brandt, S., & Lund, N. 1992, IAU Circ. 5590
Castro-Tirado, A. J., Davies, J., Brandt, S., & Lund, N. 1993, IAU Circ. 5830
Ebisawa, K., & White, N. E. 1995, IAU Circ. 6171
Foster, R. S., Waltman, E. B., Tavani, M., Harmon, B. A., Zhang, S. N., Paciesas, W. S., & Ghigo, F. D. 1996, ApJ, 467, L81
Greiner, J. 1993, IAU Circ. 5786
Greiner, J., Snowden, S., Harmon, B. A., Kouveliotou, C., & Paciesas, W. S. 1994, in AIP Conf. Proc. 304, The Second Compton Symposium, ed. C. E. Fichtel, N. Gehrels, & J. P Norris (New York: AIP), 260
Harmon, B. A., Paciesas, W. S., & Fishman, G. J. 1992, IAU Circ. 5619
Levine, A. M., Bradt, H., Cui, W., Jernigan, J. G., Morgan, E. H., Remillard, R., Shirey, R. E., & Smith, D. A. 1996, ApJ, 469, L33
Matsumoto, R., Kato, S., & Fukue, J. 1985, in Theoretical Aspects of Structure, Activity and Evolution of Galaxies, vol. 3, ed. S. Aoki, M. Iye, & Y. Yoshii (Tokyo: Tokyo Astron. Obs.), 102
Mirabel, I. F., & Rodríguez, L. F. 1994, Nature, 371, 46
Mirabel, I. F., Rodríguez, L. F., Marti, J., Teyssier, R., Paul, J., & Auriere, M. 1993a, IAU Circ. 5773
Mirabel, I. F., et al. 1993b, IAU Circ. 5830
Morgan, E. H., Remillard, R. A., & Greiner, J. 1996, ApJ, submitted
Nagase, F., Inoue, H., Kotani, T., & Ueda, Y. 1994, IAU Circ. 6094
Pooley, G. 1996, IAU Circ. 6411
Sazonov, S., & Sunyaev, R. 1996, IAU Circ. 6201
Shafer, R. A., Haberl, F., Arnaud, K. A., & Tennant, A. F. 1991, XSPEC User's Guide (ESA TM-09) (Paris: ESA)
Zhang, W., Giles, A. B., Jahoda, K., Swank, J. H., & Morgan, E. H. 1993, Proc. SPIE, 2006, 324
Zhang, S. N., Robinson, C. R., Harmon, B. A., Paciesas, W. S., & Fishman, G. J. 1996, IAU Circ. 6411
Zhang, S. N., Wilson, C. A., Harmon, B. A., Fishman, G. J., Wilson, R. B., Paciesas, W. S., Scott, M., & Rubin, B. C. 1994, IAU Circ. 6046